Journal of Thermal Analysis and Calorimetry, Vol. 90 (2007) 2, 549–555

STRUCTURAL AND THERMAL CHARACTERIZATION OF Fe(III) AND Fe(II) COMPLEXES WITH TRIDENTATE ONO PYRIDOXAL SEMICARBAZONE

Ž. K. Jaćimović[1], V. M. Leovac[2], G. Giester[3], Z. D. Tomić[4] and Katalin Mészáros Szécsényi[2]*

[1]Faculty of Metallurgy and Technology, University of Montenegro, Podgorica, Montenegro
[2]University of Novi Sad, Faculty of Sciences, Department of Chemistry, Novi Sad, Serbia
[3]Institut für Mineralogie und Kristallographie, Universität Wien, Wien, Austria
[4]'Vinča' Institute of Nuclear Sciences, Laboratory of Theoretical Physics and Condensed Matter Physics, P.O. Box 522 11001 Belgrade, Serbia

Molecular and crystal structure of diaqua-sulphato(pyridoxal semicarbazone-ONO)iron(II) and dichloroaqua(pyridoxal semicarbazone-ONO)iron(III) complexes with tridentate ONO pyridoxal semicarbazone ligand, PLSC, of formula $[Fe^{II}(PLSC)(H_2O)_2SO_4]$ and $[Fe^{III}(PLSC)(H_2O)Cl_2]Cl$ is reported. Thermal decomposition of the compounds was followed in argon and air gas carriers. The deaquation mechanism is discussed in the view of the crystal structure, emphasizing the complexity of the related parameters and processes.

Keywords: *crystal structure, deaquation mechanism, iron(II) and iron(III) complexes, pyridoxal semicarbazone thermal decomposition*

Introduction

Because of their remarkable ligation properties and simple preparation, semicarbazones represent a very interesting group of ligands to coordination chemists [1, 2]. Besides, some of these compounds possess biological activity, although generally lower in comparison with thiosemicarbazones [3]. From the point of view of the biological activity, the most known semicarbazone seems to be 5-nitrofurfural semicarbazone, which under the commercial name Furacillin® is used as a bactericide [4]. One of the new semicarbazone ligands that has recently become the subject of our interest is a tridentate ONO pyridoxal semicarbazone, PLSC. We reported the synthesis and structure of the square-pyramidal $[Cu(PLSC)Br_2]$ complex [5] and physico-chemical (magnetic, spectral and voltammetric) characteristics of some Fe(III) complexes [6, 7], among them being one of the title complexes, *viz.* $[Fe^{III}(PLSC)(H_2O)Cl_2]Cl$. In the present paper we describe the crystal and molecular structure and thermal decomposition of this compound together with the structural and thermal characteristics of the newly-prepared $[Fe^{II}(PLSC)(H_2O)_2SO_4]$ complex. The discussion of the thermal decomposition is mainly focused towards the deaquation process in view of the crystal structure, emphasizing the complexity of the related parameters. The decomposition processes above 600 K, especially in lack of coupled measurements, are too uncertain to be discussed.

Experimental

Preparation of the compounds

Green single crystals of $[Fe^{II}(PLSC)(H_2O)_2SO_4]$, **1**, were obtained by mixing of solutions of $FeSO_4$ with aqueous suspension of $PLSC{\cdot}2H_2O$ in a molar ratio of 1:1. The mixture was heated until complete dissolution of the ligand. Yield: 58%. Elemental analysis data, %, calcd. (found): C, 26.22 (26.11); H, 3.11 (2.97); N, 13.60 (13.54).

The ligand, $PLSC{\cdot}2H_2O$ (Scheme 1) and $[Fe^{III}(PLSC)(H_2O)Cl_2]Cl$, **2**, were synthesized according to the previous procedures [6].

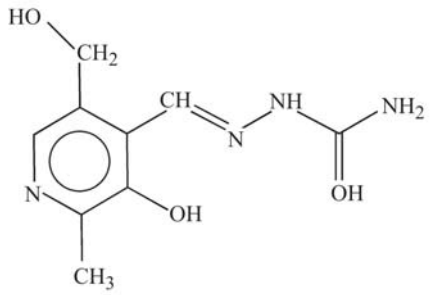

Scheme 1

* Author for correspondence: mszk@uns.ns.ac.yu

1388–6150/$20.00

Akadémiai Kiadó, Budapest, Hungary
Springer, Dordrecht, The Netherlands

Methods

Thermoanalytical measurement

Thermal analysis was performed using a DuPont 1090 TA system with sample masses of about 5 mg. Thermogravimetric measurements have been carried out in both argon and air atmospheres at a heating rate of 10 K min^{-1} in a platinum crucible, while the DSC curves were recorded with the same heating rate up to 600 K using an open aluminum pan sample holder and an empty pan as reference.

Crystal structure determination

Single-crystal X-ray diffraction analyses were performed on a Nonius KappaCCD diffractometer equipped with graphite-monochromated MoK_α radiation (λ=0.71073 Å). The structure of the compounds was solved by direct methods using SIR92 [8] and refined by a full-matrix least-squares method based on F^2 including all reflections. All non-hydrogen atoms were refined anisotropically using SHELXL-97 [9]. The methylene and aromatic C–H and N–H hydrogen atoms in **1** were located from the difference Fourier map while the methyl C–H hydrogen atoms were placed on calculated positions. In the structure **2**, hydrogen atoms bonded to N4, O3 and N2 were also located from difference Fourier map, while those bonded to C2, C6 and C9 were placed at calculated positions. It was not possible to locate hydrogen atoms bonded to O4, and the final refinement has been done without contribution of O4 hydrogen atoms. However, their presence could be inferred from the position of two chlorine atoms (Cl3) from neighboring molecules which make an angle of 109.82(4)°. The distance of these chlorine atoms from O4 are 3.016(2) and 3.066(2) Å. This geometry is expected when O4 and Cl3 are hydrogen bonded. All H atoms were refined using a riding model.

Results and discussion

The crystallographic data for **1** and **2** are summarized in Table 1. The molecular structures and the atom-numbering schemes are shown in Figs 1 and 2, respectively. Selected bond lengths and angles are given in Table 2. Crystals of **1** contain discrete neutral complex species, while in **2** the crystal structure consists of discrete complex cations and Cl^- anions. The central atoms are hexacoordinated in both molecules surrounded with ONO tridentate semicarbazone ligand. The octahedral geometry around the central Fe(III) ion in **1** is established by coordination of the sulfate ion's oxygen atom, being in *trans* position to N3 of PLSC, and by two water molecules in axial positions. Fe(II) atom in **2**

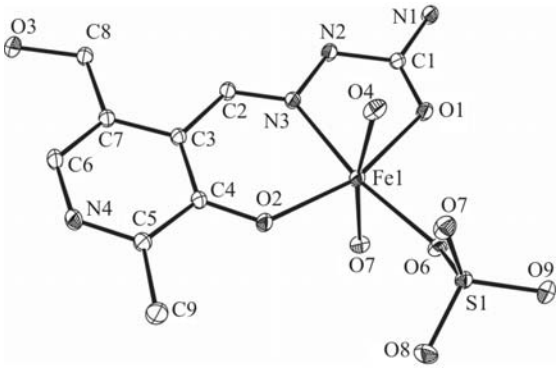

Fig. 1 Molecular structure and atom numbering scheme for complex **1**

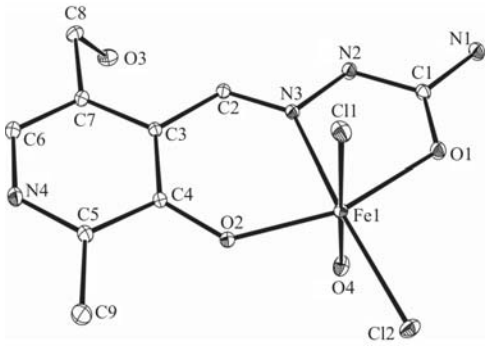

Fig. 2 Molecular structure and atom numbering scheme for complex **2**

is sited also in an octahedral surrounding with one chloride ion in *trans* position to N3. The coordination is completed by a second chloride ion and a water molecule, both of them in axial position.

In both molecules the coordination geometry corresponds to a considerably distorted octahedron. The substantial deviation from the ideal geometry in both compounds is reflected in the bite angle N3–Fe1–O1 of 75.81(5) and 75.04(5)° of the five-membered chelate ring and in the *trans* O2–Fe1–O1 angle of 159.80(5) and 155.97(5)° in **1** and **2**, respectively. The pyridoxal ring is found in its zwitterionic form with the protonated pyridine nitrogen and deprotonated phenolic hydroxyl group [10]. As shown in Table 2, the metal–donor bond lengths of Fe–ONO core in **2** are somewhat shortened compared to **1** in spite of the fact that the charge density of Fe(II) ion is lower than that of Fe(III) and the ionic radius of Fe(II) is greater. In the case of Fe(II)–N3 distance it could be explained on the basis of HSAB-principle [11–13], namely, by the greater preference of medium hard Fe(II) acid towards medium hard N base. The orientation of CH_2OH substituent of the pyridoxal moiety in **1** and **2** is different. The torsion angle of C3–C7–C8–O3 in **1** is 178.7(2)°, while in **2** the corresponding value is 59.8(2)°. The cause of this

Table 1 Selected crystallographic data of **1** and **2**

	1	**2**
Empirical formula	$C_9H_{16}FeN_4O_9S$	$C_9H_{12}Cl_3FeN_4O_4$
Formula mass	412.17	
Temperature/K	293(2)	
Crystal system	monoclinic	orthorhombic
Space group	$P2_1/n$	$P2_12_12_1$
a/Å	9.059(2)	7.073(1)
b/Å	9.443(2)	8.437(2)
c/Å	17.905(4)	25.389(5)
α/°	90	90
β/°	102.21(3)	90
γ/°	90	90
V/Å^3	1497.0(6)	1515.1(5)
Z	4	4
μ(MoK$_\alpha$)/mm^{-1}	1.204	1.543
F(000)	848	812
Reflections collected	8576	6904
Independent reflections	4534	6904
R/int	0.0166	0.0000
Data/parameters	4534/218	6904/192
Goodness-of-fit on F^2	1.116	1.227
R1 (I>2σ(I))	0.0314	0.0285
wR2 (all data)	0.1168	0.1004
$\Delta F_{maxx/min}$/e Å^{-3}	0.424/–0.661	1.287/–1.444

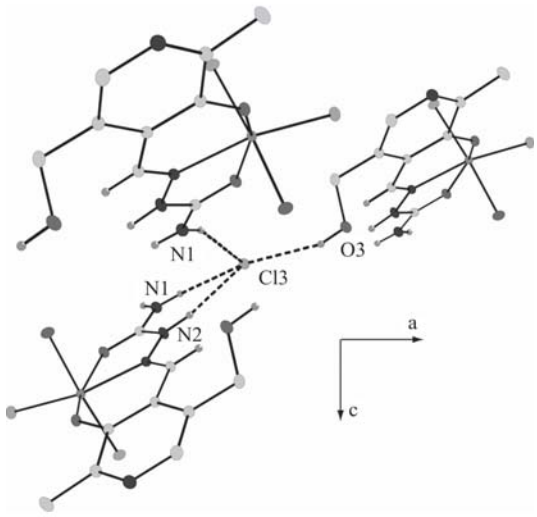

Fig. 3 Crystal packing diagram for complex **1**, with hydrogen bonds depicted by dashed lines. Hydrogen atoms not involved in hydrogen bonds are excluded for clarity

difference is not clear since the nonbonding contacts of CH_2OH are similar in both molecules (Table 2).

In the crystal of **1**, molecules are connected via O–H···O and N–H···O hydrogen bonds. Geometrical properties of these contacts are given in Table 3. The association of the molecules is determined by the presence of the sulfate oxygen atoms, placed in approximately tetrahedral arrangements.

The mode of molecular association of **1** is depicted in Fig. 3. One of the water hydrogens, H1O4, is not involved in the association of the molecules, but participates in the intramolecular hydrogen bond O4–H1O4...O7 (H···O=1.933 Å, O–H···O=161°).

Table 2 Selection of bond lengths (Å) and bond angles (°) for complexes **1** and **2**

1		**2**		**1**		**2**	
Fe1–O2	2.026(2)	Fe1–O2	1.920(1)	O5–Fe1–O4	169.35(5)	O4–Fe–Cl1	176.39(4)
Fe1–O1	2.128(1)	Fe1–O1	2.061(1)	O6–Fe1–N3	170.16(6)	N3–Fe–Cl2	169.11(4)
Fe1–N3	2.125(2)	Fe1–N3	2.196(1)	O2–Fe1–O1	159.80(5)	O2–Fe–O1	155.97(5)
O5–Fe1	2.129(1)	O4–Fe1	2.113(1)	N3–Fe1–O1	75.81(5)	O1–Fe–N3	75.04(5)
O4–Fe1	2.175(2)	Fe–Cl1	2.292(6)	O2–Fe1–N3	84.21(6)	O2–Fe–N3	81.77(5)
O6–Fe1	2.098(1)	Fe–Cl2	2.272(6)	O6–Fe1–O4	87.37(5)	Cl2–Fe–Cl1	96.68(2)
O1–C1	1.243(2)	O1–C1	1.258(2)	O1–Fe1–O4	87.21(6)	O1–Fe–Cl1	93.01(4)
N2–C1	1.376(2)	N2–C1	1.366(2)	N3–Fe1–O4	88.70(6)	N3–Fe–Cl1	92.25(4)
N3–N2	1.372(2)	N3–N2	1.362(2)	O2–Fe1–O4	95.45(6)	O2–Fe–Cl1	94.14(4)
N3–C2	1.290(2)	N3–C2	1.291(2)	O6–Fe1–O5	82.83(6)	O4–Fe–Cl2	86.29(4)
C2–C3	1.453(2)	C2–C3	1.458(2)	O1–Fe1–O5	89.48(6)	O1–Fe–O4	84.51(5)
C4–C3	1.426(2)	C4–C3	1.415(2)	N3–Fe1–O5	100.30(6)	O4–Fe–N3	84.58(6)
O2–C4	1.300(2)	O2–C4	1.307(2)	O2–Fe1–O5	91.16(6)	O2–Fe–O4	87.12(5)
O3–C8	1.408(2)	O3–C8	1.433(2)	O2–Fe1–O6	105.14(5)	O2–Fe–Cl2	103.71(4)
				O6–Fe1–O1	94.98(5)	O1–Fe–Cl2	98.19(4)

Table 3 Geometry of the significant intermolecular contacts in **1**

D–H	A	H···A/Å	D–H···A/°
O3–H1O3	$O9^{I}$	1.83	172
O4–H2O4	$O3^{II}$	1.94	172
O5–H1O5	$O2^{III}$	2.04	158
O5–H2O5	$O8^{IV}$	1.78	177
N4–H1N4	$O7^{V}$	1.99	158
N2–H1N2	$O8^{VI}$	1.96	158
N1–H1N1	$O9^{VII}$	2.13	150
N1–H2N1	$O9^{VIII}$	2.26	159

Symmetry codes:
I=1/2+*x*, 1/2–*y*, 1/2+*z*; II=2–*x*, 1–*y*, 1–*z*; III=1–*x*, –*y*, 1–*z*; IV=2–*x*, –*y*, 1–*z*; V=*x*, 1+*y*, *z*; VI=1/2–*x*, 1/2+*y*, 1/2–*z*; VII=*x*, 1+*y*, *z*; VIII=1/2–*x*, 1/2+*y*, 1/2–*z*

Table 4 Geometry of the significant intermolecular contacts in **2**

D–H	A	H···A/Å	D–H···A/°
O3–H1O3	$Cl3^{I}$	2.41	159
N1–H1A	$Cl3^{II}$	2.43	156
N1–H1B	Cl3	2.79	145
N2–H1N2	Cl3	2.27	162

Symmetry codes: I=–*x*, 1/2+*y*, 1/2–*z*; II=1–*x*, –1/2+*y*, 1/2–*z*

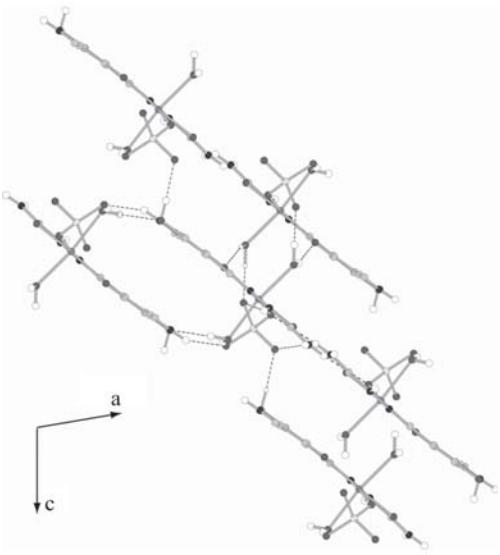

Fig. 4 Crystal packing diagram for complex **2**, with hydrogen bonds depicted by dashed lines. Hydrogen atoms not involved in hydrogen bonds are excluded for clarity

The packing of molecules in the crystal of **2** is governed by the presence of free chloride ions which accept hydrogen bonds from the three surrounding molecules (Fig. 4). The geometry of the hydrogen bonds is given in Table 4.

It is interesting to note that in the crystal structure of **2** the two chlorine atoms, coordinated to Fe(III) in equatorial and axial position, are not involved in the association of molecules in the unit cell. It is somewhat unexpected as the chlorine is known to be a good acceptor for hydrogen bonds. In the crystal structure of a structurally similar compound *cis*-aqua-dichloro-(pyridoxal-isonicotinoyl-hydrazone-N,O,O')-iron(III) chloride monohydrate [14], where the coordination environment of Fe(III) is very similar to **2**, the axially coordinated chlorine takes part in the association of the molecules.

Thermal analysis

The thermal decomposition curves of **1** and **2** are presented in Figs 5 and 6. The decomposition temperature does not depend on the atmosphere. The course of the decomposition of both compounds is different in argon and air gas carriers. In argon it is not complete up to 1000 K neither for **1** nor for **2**. In air the decomposition of **1** above 600 K is accompanied with uncontrolled – probably oxidation – processes which were observed in the case of other sulfur containing complexes in a platinum crucible [15, 16]. Thus, our discussion on thermal decomposition shall be reduced to about 600 K. In argon **1** is stable after dehydration in a temperature range of about 60 K. The decomposition of **2** is continuous in the whole temperature range.

As both complexes are hydrates, the first decomposition step is their deaquation. According to the crystal structure, water molecules belong to the inner coordination sphere. Thus, in the accordance with the crystal structure, the deaquation temperature is rather high:

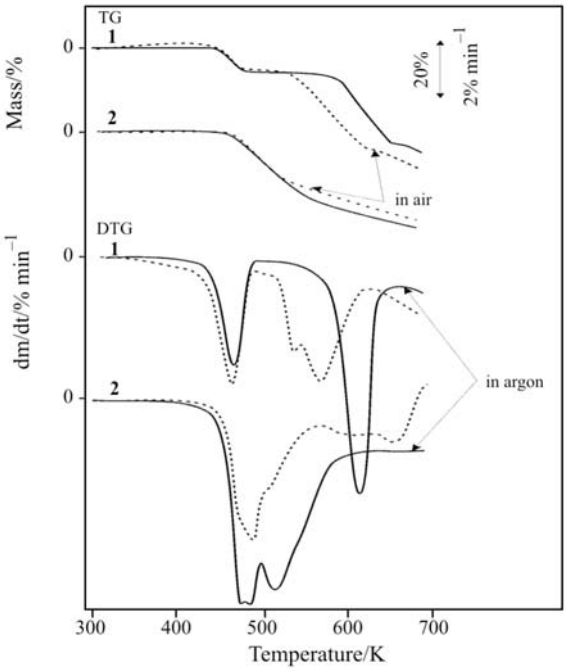

Fig. 5 TG-DTG curves of the compounds

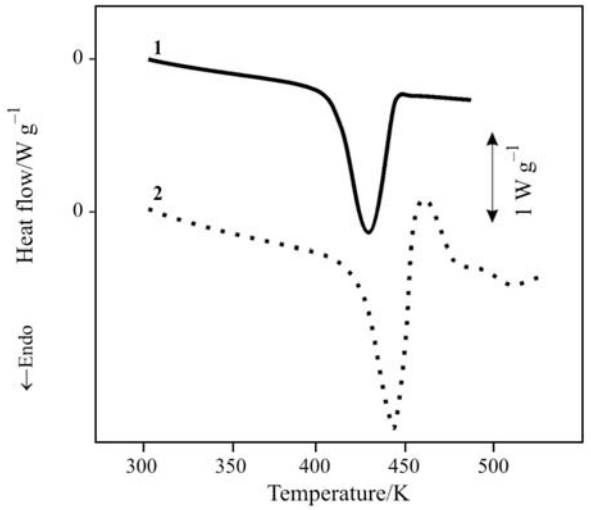

Fig. 6 DSC curves of the compounds

both compounds release water around 450 K (450 K for **1** and 440 K for **2**). To our knowledge there are no literature data on the mechanism of the dehydration, discussed in the view of the crystal structure. Thermal data on dehydration of isostructural compounds [17–20] usually refer to a similar course of their decomposition and vice versa. The complexity of the dehydration of the compounds with a different structure and different number of water molecules [21, 22] is diverse. Sometimes it takes place in one step, sometimes the DTG curves refer to a multi-step dehydration. The onset temperature of the dehydration of *dl*-lactates of transition metals and alkaline earth metal hydrates with different number of H_2O does not show any pattern. The dehydrations proceed without intermediate formation [23]. The six lattice water molecules of the tris(ethylendiamine)cobalt(III) 1.5 squarate hexahydrate, molecule with known crystal structure, depart in two hardly distinguishable step in a temperature range of 50–153°C, i.e., in a relatively wide interval and up to a significantly higher temperature than the boiling point of water [24]. In $[Ni(acs)(H_2O)_4]$, acs=acesulfamato ion, Ni(II)–O(H_2O) distances are O2(O2')–Ni1 2.0481(13) and O3(O3')–Ni1 2.0568(11) Å. The hydrogen atoms of the two aqua ligands are involved in inter- and intramolecular hydrogen bonding. However, these interactions differ from each other as in involved atoms so in interatomic distances. Thus, even the small difference of 0.009 Å in Ni(II)–O(H_2O) distances together with hydrogen bonds is noticeable as an asymmetry in DTG curve's shape [25]. Its deaquation takes place in a temperature range of 105–175°C. In the analogous cobalt(II) complex the corresponding Co(II)–O(H_2O) bond lengths differ up to 0.02 Å [26]. All four water molecules take part in inter- and intramolecular hydrogen bonds with different interatomic distances. Most probable these differences are visible in clearly distinguishable deaquation steps: three water molecules depart in an 86–148°C temperature range, while the last one in the range of 160–190°C [25].

The interatomic Fe(III)–O(H_2O) distances in **1** are 2.129(1) and 2.175(2) Å, respectively, while in **2** Fe(II)–O(H_2O) the distance amounts 2.113(1) Å, i.e., they are close, referring to about the same bonding energy of water molecules which manifests in the close deaquation temperatures. The evaporation of water molecules in **1** takes place in a narrow temperature range of 50 K, with almost a symmetrical DTG curve, referring to a one-step deaquation, in spite of the fact that there is a difference of about 0.05 Å in Fe(III)–O(H_2O) bond lengths. The coulombic potential energy terms are inversely proportional to the interatomic distances [27]. As a consequence, shorter bond length should refer to a stronger bonding energy. This should be reflected at least in an asymmetrical deaquation curve of **1**. However the deaquation process depends also on the intermolecular interactions of the leaving fragment. Having in mind the tendency of H_2O to form strong hydrogen bonds, it is possible that difference in the Fe–O bonding energies are compensated to some extent by the different hydrogen bond energies of the two water molecules which lead to the one-step deaquation of **1**. Besides, the deaquation usually leads to the change of the coordination mode of the central atom and is connected to LFSE (ligand field stabilization energy). This may favor or hinder the deaquation. In addition, during the deaquation, anion(s) may occupy the place of the departing water molecules. In that case, the lattice energy component of the activation energy also may favor or hinder the diffusion of water molecules through the lattice [28].

In crystals there are many interactions affecting the evaporation of the solvent molecules, like their departure through the capillaries of the grain between interface→grain boundary, grain boundary→sample surface, sample surface→surrounding which are usually the rate determining steps. Thus, in order to understand the desolvation processes, it would be necessary to make a correlation between the processes which may affect the loss of solvent molecules during the thermal treatment (bonding energy, diffusion, degree of dispersity of the solid particles or/and the degree of crystallinity of the sample, etc.) with the crystal data (bond length, hydrogen bonds, inter- and intramolecular interactions in the crystal, unit cell volume, density, etc.) which may influence the desolvation. At the moment, we do not have enough data to analyze all the above mentioned corresponding interactions. The TA data suggest that the interatomic distances, and accordingly, the different bonding energies, do not affect the mechanism of dehydration in this particular case.

In the case of **1** the anhydrous sample in argon is relatively stable. The experimentally determined water content (8.7%) agrees with the theoretical one (8.75%). The following decomposition steps are almost inseparable avoiding the proposition of an acceptable decomposition mechanism. According to the decrease in mass, the next step may correspond to H_2SO_4 elimination (23.80% calcd., 24% exp.) but the decomposition mechanism, proposed on the basis of the mass loss not always corresponds to the real processes. In **2** the step overlapping the dehydration is most likely the departure of a HCl molecule, which was observed earlier [29, 30], especially taking into account that one chloride ion in the complex belongs to the outer coordination sphere. The calculated mass loss for $\Delta m(H_2O+HCl)$ amounts 13.61% while the mass loss to the minimum in DTG curve is 12% which may support the proposition of the simultaneous departing of H_2O and HCl. In order to obtain more reliable data on the decomposition mechanism coupled EGD or EGA techniques should be applied [31–34].

No melting of the compounds was observed during the heating. The decomposition of both **1** and **2** begins with an endothermic deaquation (Fig. 6) which is in the case of **2** followed by a small exothermic peak, probably being a consequence of structural changes in the molecule [35], but is compensated with other decomposition processes.

Conclusions

The deaquation of the complexes is different, most probably due to different interactions inside of the crystals. The one-step dehydration mechanism in **1** might be interpreted taking into account that the different bonding energies due to different bond lengths are partly compensated by intermolecular hydrogen bonded Fe(III)–O4(H_2O) water molecules. On this basis one can state that the diffusion of the molecules through the crystal is not the rate determining step. To understand the desolvation (deaquation) mechanism, taking into account the crystal structure of the compounds, additional data are needed which relate the thermal desolvation pattern with the crystal structure, in the first place that of isostructural compounds.

The dehydrated **1** is stable in about 60 K temperature range. On the basis of the mass loss the step following the deaquation may be the departure of H_2SO_4 (23.80% calcd., 24% exp.). The deaquation of **2** is accompanied most probable by evolution of HCl. The mass loss up to the minimum of DTG (about 500 K) agrees with evaporation of an H_2O and an HCl molecule (13.61% calcd., 12% exp.), in the accordance with our earlier experiences.

Supplementary material

A full list of crystal data and refinement of **1** and **2** has been deposited at the Cambridge Crystallographic Data Centre, CCDC No. 627019 and 627020, respectively.

Acknowledgements

The work was financed by the Ministry for Science and Environmental Protection of the Republic of Serbia (Grant No. 142028) and the Provincial Secretariat for Science and Technological Development of Vojvodina.

References

1 S. B. Padhye and G. B. Kaufman, Coord. Chem. Rev., 63 (1985) 127.
2 J. S. Casas, M. S. Garcia-Tasende and J. Sordo, Coord. Chem. Rev., 209 (2000) 197.
3 H. Beraldo and D. Gambino, Mini Rev. Med. Chem., 4 (2004) 159.
4 M. D. Mashkovskii, Lekartstvenie sredstva, Meditsina, Moscow 1984.
5 D. Poleti, Lj. Karanović, V. M. Leovac and V. S. Jevtović, Acta Cryst., C59 (2003) m73.
6 V. S. Jevtović, Lj. S. Jovanović, V. M. Leovac and L. J. Bjelica, J. Serb. Chem. Soc., 68 (2003) 929.
7 Lj. S. Jovanović, V. S. Jevtović, L. J. Bjelica and V. M. Leovac, J. Serb. Chem. Soc., 70 (2005) 187.
8 A. Altomare, G. Cascarano, C. Giacovazzo, A. Guagliardi, M. C. Burla, G. Polidori and M. Camalli, J. Appl. Crystallogr., 27 (1994) 435.
9 G. M. Sheldrick, SHELXL-97, Program for Refinement of Crystal Structures, University of Göttingen, Germany 1997.
10 M. Belicchi Ferrari, G. Gasparri Fava, C. Pelizzi, P. Tarasconi and G. Tosi, J. Chem. Soc. Dalton Trans., (1986) 2455.
11 R. G. Pearson, J. Am. Chem. Soc., 85 (1963) 3533.
12 R. G. Pearson and J. Songstad, J. Am. Chem. Soc., 89 (1967) 1827.
13 T.-L. Ho, Chem. Rev., 75 (1975) 1.
14 T. B. Murphy, N. J. Rose, V. Schomaker and A. Aruffo, Inorg. Chim. Acta, 108 (1985) 183.
15 K. Mészáros Szécsényi, V. M. Leovac, Ž. K. Jaćimović and G. Pokol, J. Therm. Anal. Cal., 74 (2003) 943.
16 Atlas of Thermoanalytical Curves, G. Liptay (Ed.), Vol. 3, No.160, Akadémiai Kiadó, Budapest and Heyden and Sons, London 1974.
17 T. Premkumar and S. Govindarajan, J. Therm. Anal. Cal., 79 (2005) 115.
18 T. Premkumar and S. Govindarajan, J. Therm. Anal. Cal., 84 (2006) 395.
19 D. Czakis-Sulikowska, J. Radwańska-Doczekalska, A. Czilkowska and J. Gołuchowska, J. Therm. Anal. Cal., 78 (2004) 501.
20 W. Ferenc, B. Cristóvão and J. Sarzińsky, J. Therm. Anal. Cal., 86 (2006) 783.

21 P.M. Takahashi, A. V. G. Netto, A. E. Mauro and R. C. G. Ferm, J. Therm. Anal. Cal., 79 (2005) 335.
22 A. A. M. Aly, A. H. Osman, N. Abo El-Maali and G. A. A. Al-Hazmi, J. Therm. Anal. Cal., 75 (2004) 159.
23 R. K. Verma, L. Verma, M. Chandra and A. Bhushan, J. Therm. Anal. Cal., 80 (2005) 351.
24 O. Z. Yesilel, H. Ölmez and S. Soylu, Trans. Met. Chem., 31 (2006) 396.
25 H. Icbudak, E. Adiyaman and N. Cetin, Trans. Met. Chem., 31 (2006) 666.
26 H. Icbudak, A. Bulut, N. Cetin and C. Kazak, Acta Cryst., C61 (2005) m1.
27 L. Pauling, J. Phys. Chem., 58 (1954) 662.
28 J. Casabó, T. Flor, F. Teixidor and J. Ribas, Inorg. Chem., 25 (1986) 3166.
29 K. Mészáros Szécsényi, V. M. Leovac, Ž. K. Jaćimović, V. I. Češljević, A. Kovács and G. Pokol, J. Therm. Anal. Cal., 66 (2001) 573.
30 V. M. Leovac, K. Mészáros Szécsényi, Lj. S. Vojinović Ješić, V. I. Češljević, S. Markov and T. Wadsten, J. Therm. Anal. Cal., 89 (2006) 379.
31 M. Krunks, J. Madarász, T. Leskelä, A. Mere, L. Niinistö and G. Pokol, J. Therm. Anal. Cal., 72 (2003) 497.
32 R. Mrozek-Łyszczek, J. Therm. Anal. Cal., 78 (2004) 473.
33 J. Madarász, M. Krunks, L. Niinistö and G. Pokol, J. Therm. Anal. Cal., 78 (2004) 679.
34 D. Czakis-Sulikowska, J. Radwańska-Doczekalska, A. Czylkowska, J. Gołuchowska and R. Mrozek-Łyszczek, J. Therm. Anal. Cal., 78 (2004) 501.
35 H. A. El-Boraey, J. Therm. Anal. Cal., 81 (2005) 339.

Received: November 20, 2006
Accepted: April 24, 2007

DOI: 10.1007/s10973-006-8267-x